DEGREE PROJECT IN TECHNOLOGY,
SECOND CYCLE, 30 CREDITS
STOCKHOLM, SWEDEN 2022

Prediction of Detonation Performance of CHNO Explosives

KTH Thesis Report

Anders Abrahamsson

KTH ROYAL INSTITUTE OF TECHNOLOGY
Molecular Science and Engineering

Authors

Anders Abrahamsson aabraha@kth.se
Molecular Science and Engineering
KTH Royal Institute of Technology

Place for Project

Stockholm, Sweden
KTH Royal Institute of Technology, Department of Physical Chemistry

Examiner

Prof. Tore Brinck Stockholm, Sweden
KTH Royal Institute of Technology, Department of Physical Chemistry

Supervisors

Prof. Tore Brinck

Stockholm, Sweden

KTH Royal Institute of Technology, Department of Physical Chemistry

Victor Björkgren

Karlskoga, Sweden

Saab Dynamics

Abstract

Producing new energetic materials is expensive. This work aims to develop a method of estimating the Chapman-Jouget detonation pressure and the detonation velocity of potential new CHNO explosives. This would allow choosing the most promising candidates for synthesis and testing thus avoiding wasting resources. This method utilizes density functional theory (DFT) and the electrostatic potential to estimate heats of formation and crystal densities. The calculations were performed on traditionally used explosives and the calculated detonation pressures and detonation velocities showed good accordance with experimental data. The calculated detonation pressures fell within $\pm 10\%$ and the detonation velocities within $\pm 5\%$ of experimental data.

Keywords

Master thesis, Detonation pressure, Detonation velocity, Electrostatic potential, Crystal density, Heat of formation, Energetic material

Abstrakt

Produktion av nya energetiska material är dyrt. Målet med detta arbete är att utveckla en metod som uppskattar Chapman-Jouget detonationstrycket och detonationshastigheten hos nya CHNO-sprängämnen. En sådan metod möjliggör valet att bara syntetisera och testa de mest lovande kandidaterna som nya energetiska material, därmed undviks resursslösande arbete. Den här metoden använder sig av density functional theory (DFT) och den elektrostatiska potentialen till att uppskatta bildningsentalpier och kristalldensiteter. Beräkningarna gjordes på traditionella sprängämnen och de beräknade detonationstrycken och detonatioshastigheterna visade bra överensstämmelse med experimentell data. Detonationstrycken hamnade inom $\pm 10\%$ och detonatioshastigheterna inom $\pm 5\%$ av experimentell data.

Nyckelord

Master examensarbete, Detonationstryck, Detonationshastighet, Elektrostatisk potential, Kristalldensitet, Bildningsentalpi, Energetiska material

Acknowledgements

I wish to thank my supervisor and examiner Prof. Tore Brinck for all the guidance, advice and support given to me during this thesis.

I would also like to thank my supervisor Victor Björkgren and the people at Saab Dynamics for giving me the opportunity to explore the world of quantum chemistry and energetic materials.

Acronyms

DFT Density Functional Theory

ESP Electrostatic Potential

P_{CJ} Chap-Jouget Detonation Pressure

D Detonation Velocity

TNT 2,4,6-Trinitrotoluene

RDX 1,3,5-Trinitroperhydro-1,3,5-triazine

HMX 1,3,5,7-tetranitro-1,3,5,7-tetrazocane

CL20 Hexanitrohexaazaisowurtzitane

FOX7 1,1-diamino-2,2-dinitroethylene

PETN Pentaerythritol tetranitrate

DOTZ 1,4,2,3,5,6-dioxatetrazinane

ONC Octanitrocubane

Contents

1 Introduction

The need for green energetic materials continues to grow. Due to the better understanding of substances toxicity profiles over the last few decades it has resulted in increasing regulation regarding energetic materials. This leads to the phasing out of traditional energetic materials. Historically, the energetic materials were chosen based on their performance and reliability. The toxicity was not taken into consideration, however, it is both an environmental and occupational health concern [2]. Although primary explosives typically consist of more toxic components, such as lead in lead azide, the production of secondary explosives is several orders of magnitude greater than the production of primary explosives [3]. The detonation products of common secondary explosives such as RDX (1,3,5-Trinitroperhydro-1,3,5-triazine) and HMX (1,3,5,7-tetranitro-1,3,5,7-tetrazocane) contain carbon monoxide which is not considered as toxic as lead, however, still a cause of concern.

New energetic materials should ideally have no, or minimal amount of, hazardous components in their life cycle while maintaining, or exceed, the performance when comparing with conventional energetic materials in their respective field.

Producing and testing new energetic materials is both time-consuming and expensive [7]. To avoid wasting resources on bad candidates, a model predicting the properties of an energetic material accurately would be an ideal choice. This would allow for screening a large number of new energetic material candidates and only choosing the most promising ones for synthesis and testing.

This work investigates whether a quantum chemical model can be used to predict the detonation pressure and detonation velocity of secondary CHNO-explosives by comparing predicted detonation properties of some traditional energetic materials with their experimentally measured ones.

2 Background

2.1 Detonation Properties

Two properties of interest regarding detonation of an energetic material are the Chapman-Jouguet detonation pressure, P_{CJ}, and the detonation velocity, D. The two go hand in hand and can be estimated by empirical equations given the heat of detonation, the stoichiometry of the detonation products and the density of the energetic material as shown by Keshavarz et al.[7] [6]. They proposed two new simple methods of estimating the P_{CJ} and D, which can be seen in eq. (1) and eq. (2) respectively.

$$P_{CJ} = 15.88\alpha(MQ_{Det})^{1/2}\rho_0^2 - 11.17 \tag{1}$$

$$D = 5.468\alpha^{1/2}(MQ_{Det})^{1/4}\rho_0 + 2.045 \tag{2}$$

2.2 Parameters

The proposed equations use four parameters in total. Three of them are connected to the stoichiometry of the detonation reaction. The first parameter, α is the amount of gas in moles produced per gram of explosive. The second parameter, M, is the average molecular weight of the gasses produced. The third parameter, Q_{Det} , is the heat of detonation and is defined as in eq. (3), in cal/g. It utilizes the heat of formation of the explosive and its detonation products to calculate the amount of heat released upon detonation [7].

$$Q_{Det} \cong -\frac{[\Delta H_f(Products) - \Delta H_f(Explosive)]}{M_W(Explosive)} \tag{3}$$

Since the stoichiometry of the detonation reaction is needed in order to calculate the P_{CJ} and D. The decomposition products need to be determined. This remains an unresolved problem for more complex elemental compositions of energetic materials. However, Keshavarz et al. proposed a procedure, based on thermochemical calculations of 34 CHNO explosives, that approximates the stoichiometry of the decomposition products only using the molecular formula of the energetic material. A schematic view of this procedure can be seen in figure

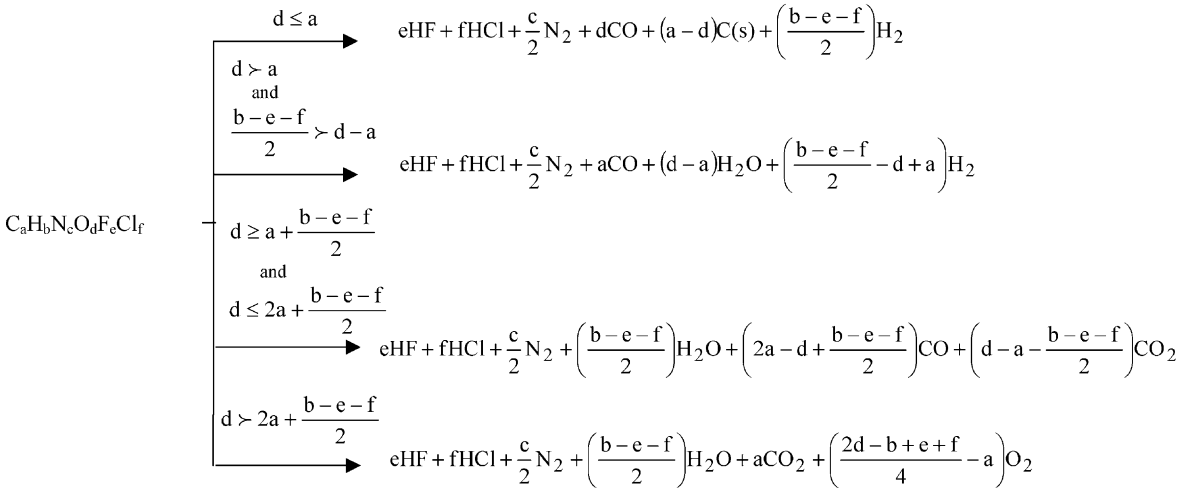

Figure 2.1: *Products*

2.1.

2.3 Electrostatic Potential

The electrostatic potential, ESP, is defined as equation 4 and is produced by the electrons and nuclei of the molecule. It is typically evaluated at the 0.001 electrons/bohr^3 contour of the electron density. By using surface descriptors of the electrostatic potential surface such as the total variance, σ^2_{tot}, and the electrostatic balance , v, intermolecular interactions can be modeled and some material properties can be predicted [11][4]. σ^2_{tot} and v are defined as eq. (5) and eq. (6) respectively.

$$\mathbf{V(r)} = \sum_A \frac{Z_A}{\mid \mathbf{R}_A - \mathbf{r} \mid} - \int \frac{\rho(\mathbf{r}')d\mathbf{r}'}{\mid \mathbf{r}' - \mathbf{r} \mid} \tag{4}$$

$$\sigma^2_{tot} = \sigma^2_+ + \sigma^2_- \tag{5}$$

$$v = \frac{\sigma^2_+ \, \sigma^2_-}{(\sigma^2_+ + \sigma^2_-)^2} \tag{6}$$

Where σ^2_+ and σ^2_- are defined as follows;

$$\sigma^2_+ = \frac{1}{m}\sum_{i=1}^{m}\left[V_S^+(\mathbf{r}_i) - \overline{V}_S^+\right]^2 \qquad \sigma^2_- = \frac{1}{m}\sum_{i=1}^{m}\left[V_S^-(\mathbf{r}_i) - \overline{V}_S^-\right]^2$$

2.4 Heat of Sublimation

Because the explosives examined in this work exist in their solid-state in practical use, the heat of sublimation needs to be accounted for. If the heat of formation in the gas phase and the heat of sublimation is known, then the heat of formation in the solid phase can be obtained through eq. (7). Since the heat of formation of a compound, in either gas, liquid or solid, may not be available from experimental data another route must be taken. A computational procedure developed by Politzer et al. allows for prediction of standard gas phase heats of formation by including empirical atomic correction terms to the ΔH_r of the reaction of the compound from its elements. The electrostatic potential is then used to estimate the heats of sublimation and vaporization. This method produced an absolute average deviation from experimental data in heats of formation of 3.8 kcal/mol in their solid phase and 2.8 kcal/mol for the heats of sublimation. This method used density functional theory, DFT, with the functional B3PW91 and the 6-31G** basis set. The equation used to estimate the heat of sublimation can be seen in eq. (8) [11].

$$\Delta H_f^o(solid) = \Delta H_f^o(gas) - \Delta H_{sub}^o \tag{7}$$

$$\Delta H_{sub}^o = 4.4307 \times 10^{-4} A_S^2 + 2.0599\sqrt{v\sigma_{tot}^2} - 2.4825 \tag{8}$$

2.5 Density

Lastly is the loading density of the explosive material, ρ_0. Politzer et al. developed an equation, see eq. (9), using the surface descriptors of electrostatic potential surface and volume of an isolated molecule, V_M. The equation produced predicted crystal densities where 78% are within $0.050\frac{g}{cm^3}$ from experimental values and 50% are within $0.030\frac{g}{cm^3}$ [12].

$$\rho_0 = 0.9183\left(\frac{M_W}{V_m}\right) + 0.0028\left(v\sigma_{tot}^2\right) + 0.0443 \tag{9}$$

3 Method

All molecules were optimized and underwent frequency calculations, using $Gaussian16$, in order to obtain the sum of the electronic and thermal enthalpies. The results were checked for imaginary frequencies and were not included if an imaginary frequency was present. This was performed using three levels of theory. Firstly, the functional B3PW91 with the basis-set 6-31G** was used in order to compare the calculated heats of formation to previous work by Politzer et al. Then the same calculations were performed using the M06-2X functional also with the 6-31G** basis-set. Lastly, the calculations were performed using the M06-2X functional and the Jun-cc-pVTZ basis-set. This was done in order to compare how the accuracy of the level of theory affects the predicted detonation properties. This was performed on six commonly used energetic materials with well established experimental data, namely TNT (2,4,6-Trinitrotoluene), RDX (1,3,5-Trinitroperhydro-1,3,5-triazine), HMX (1,3,5,7-tetranitro-1,3,5,7-tetrazocane), CL20 (Hexanitrohexaazaisowurtzitane), FOX7 (1,1-diamino-2,2-dinitroethylene) and PETN (Pentaerythritol tetranitrate). Their structures are shown in figure (3.1) and their experimental data are shown in table 1.

The heat of formations in the gas phase were obtained by calculating the heat of reaction, ΔH_r, of each of the compounds from its pure elements, i.e C(s), H_2 (g), N_2 (g) and O_2 (g). The heat of sublimation of C(s) used in the calculations was 171.18 kcal/mol [8]. For the B3PW91/6-31G** level of theory, the procedure followed that of Politzer's group where atomic correction terms were added to the ΔH_r to obtain a more accurate gas heat of formation [11]. This was not performed for the M06-2X/6-31G** and M06-2X/Jun-cc-pVTZ level of theory. The crystal densities were calculated using eq. (9)[12].

The electrostatic potential and the surface descriptors were obtained using the HS95 code developed by Prof. T. Brinck.

When all parameters were obtained for each conformer of each molecule they were used as input into eq. (1), eq. (2) and EXPLO5. The calculated detonation pressures and detonation velocities were then compared with experimental data. The experimental data is shown in table 3.

Table 1. *Experimental data of traditional energetic materials. (Obtained from LLNL Explosives Handbook [6] if not else stated)*

Experimental data

Substance	$\mathrm{HoF}_s[\frac{kcal}{mol}]$	$\rho_0[\frac{g}{cm^3}]$	$\mathrm{Q}_{Det}[\frac{cal}{g}]$	$\mathrm{P}_{CJ}[kbar]$	Detonation velocity $[\frac{m}{s}]$	TMD $[\frac{g}{cm^3}]$
TNT	-16.0	1.630	1020	210	6930	1.654
RDX	14.71	1.767	1420	338	8700	1.806
HMX	17.93	1.890	1370	390	9110	1.905
CL-20	108.6^a	2.040^a	1563^b	420^a	9380^a	-
FOX-7	-28.8^c	1.880^d	-	340^d	8870^d	1.894^d
PETN	-128.7	1.770	1370	335	8260	1.780
Comp B-3	1.15	1.720	1120	287	7890	1.742
Cyclotol	3.21	1.760	-	316	8300	1.770
Octol	2.78	1.810	-	342	8480	1.843

[a] [17]
[b] [16]
[c] [13]
[d] [1]

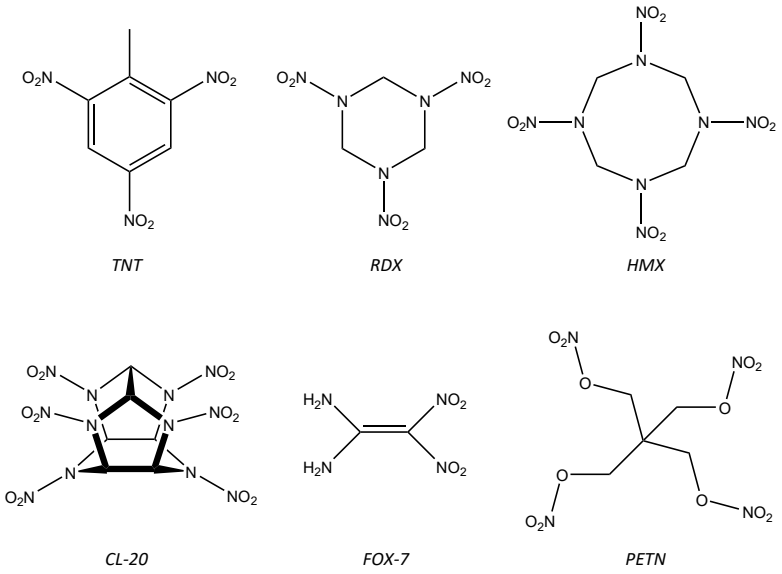

Figure 3.1: *Molecular structures of the traditional energetic materials.*

3.1 Conformers

When optimizing a molecule it is important to note that the obtained optimized structure is not guaranteed to be a global potential energy minima. Depending on the structure, there can be several local potential energy minimas close in energy. It is also difficult to prove mathematically that the entire potential energy surface has been scanned and that all local potential energy minimas have been found. When some local minimas have been found it is not certain that they exist in the solid state. Conformers that exist in crystalline form can be determined by X-ray diffraction. However, this requires the material to be synthesized beforehand. A part of this work is therefore to check a couple of conformers of the same molecule to investigate how much this affects the estimated P_{CJ} an D. In total five conformers of RDX, three conformers of HMX, three conformers of CL20, two conformers of TNTNB and one conformer of FOX-7, TNT and PETN each were calculated and analyzed. The RDX conformers were taken from previous work by Molt et al where two conformers, α and β, exist in crystalline form [10]. The conformers of RDX used in this work are illustrated in figure 3.2. Molt has also investigated several HMX conformers from three that were chosen for this purpose. Two of those conformers exist in crystalline form as β- and δ-HMX [9][13].

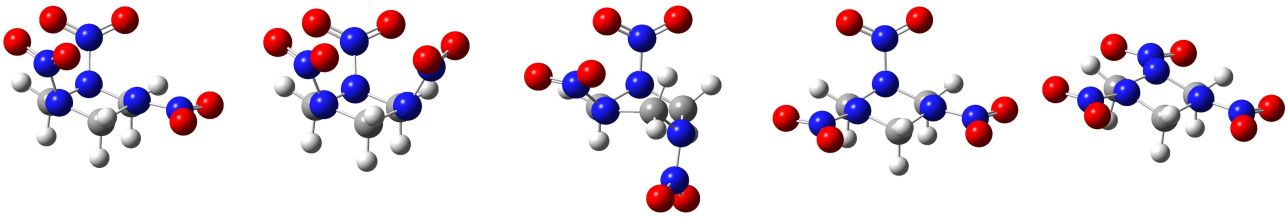

Figure 3.2: *RDX Conformers.*

3.2 Mixtures

Energetic materials do not only consist of pure substances, there are mixtures as well. Some common mixtures are Comp B-3, Cyclotol and Octol. The first two are mixtures of RDX/TNT in ratios of 60/40 $wt\%$ and 75/25 $wt\%$ respectively. Octol is a HMX/TNT mixture with a ratio of 75/25 $wt\%$. The components of each mixture was assumed to not interact with each other so the α, M, Q_{Det} and ρ_0 was calculated by weighting each property by their $wt\%$ or equivalent $mol\%$.

3.3 New Candidates

After the results of the traditional energetic materials were evaluated, three new candidates were chosen to estimate their detonation properties. The new candidates are DOTZ (1,4,2,3,5,6-dioxatetrazinane), Comp 76 and ONC (Octanitrocubane), their structures are shown in figure (3.3). DOTZ was chosen due to it containing only H, N and O. Comp 76 was chosen due to its N-hetero cycle and azide groups. Lastly, ONC was chosen due to its cage structure[1][14][5]. They underwent the same procedure as the traditional ones except being calculated using EXPLO5.

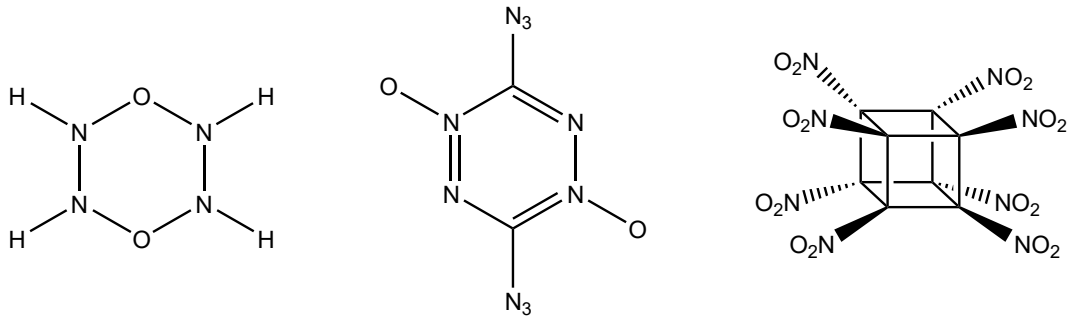

Figure 3.3: *Molecular structures of the new candidates.*

4 Results

4.1 Heat of Formation

The calculated heats of formation of the traditional energetic materials at the different levels of theory can be seen plotted in figure (4.1) together with the experimentally obtained heat of formation. From this graph it can be seen that M06-2X/Jun-cc-pVTZ produced the most accurate results when compared with experimental data. B3PW91/6-31G** is less accurate and fluctuates more in terms of over- and under estimating the heats of formations. Lastly, M06-2X/6-31G** is the least accurate level of theory when estimating heats of formation according to these results.

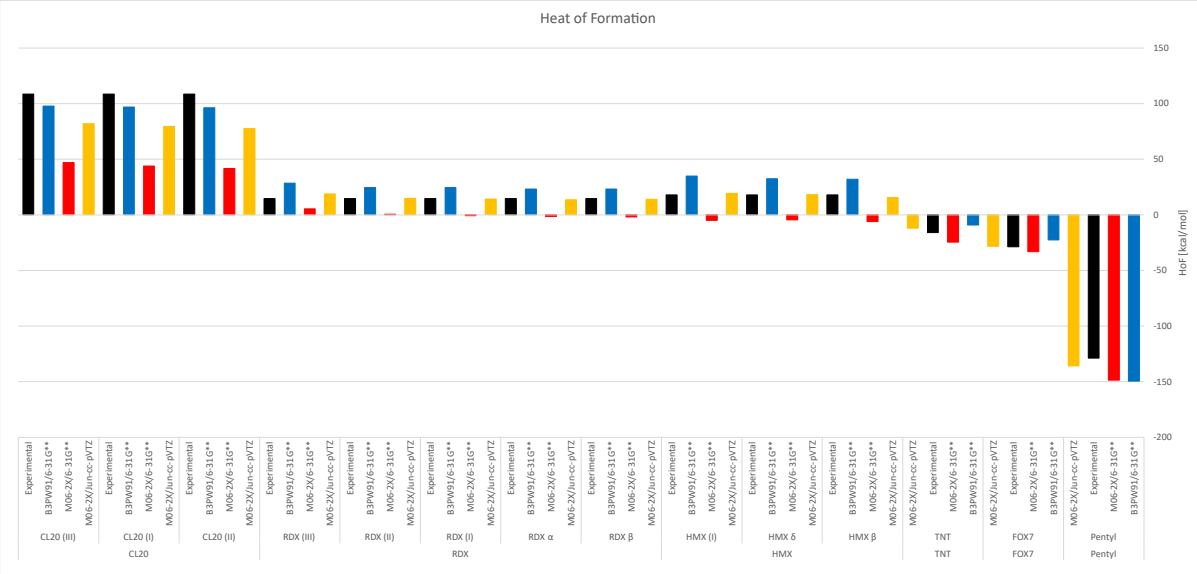

Figure 4.1: *Calculated heats of formation of the traditional energetic materials using B3PW91/6-31G** (blue), M06-2X/6-31G** (red) and M06-2X/Jun-cc-pVTZ (yellow) and their respective experimentally obtained heats of formation (black).*

4.2 Density

The estimated crystal densities of the traditional energetic materials are compared with their respective TMD in figure (4.2). Since the Jun-cc-pVTZ basis-set is not parameterized in the HS95 code, the surface descriptors used in the calculation of the crystal densities were taken from the M06-2x/6-31G** level of theory. This resulted in the calculated crystal densities from M06-2X/6-31G** and M06-2X/Jun-cc-pVTZ being identical. The average difference between the calculated crystal density with B3PW91/6-31G** and the TMD was an underestimation by 29 mg, while the M06-2X functional produced an average underestimation of 13 mg.

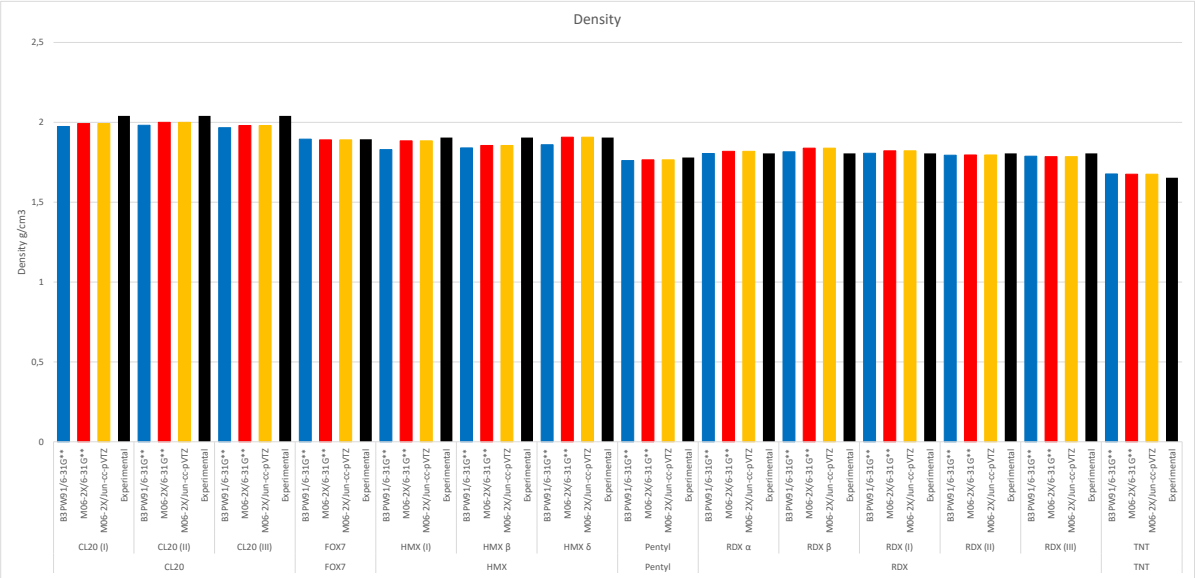

Figure 4.2: *Calculated crystal densities of the traditional energetic materials using B3PW91/6-31G** (blue), M06-2X/6-31G** (red) and M06-2X/Jun-cc-pVTZ (yellow) and their respective TMD (black).*

4.3 Detonation Pressure

The resulting calculated P_{CJ} and D using eq. (1) and eq. (2) , are shown in table 2 and table 3 respectively together with the results from EXPLO5. This is also visualized in figure (4.3a) and (4.3b). When comparing the calculated P_{CJ} using eq. (1) and EXPLO5 with the experimental value of P_{CJ} for the pure substances, it can be seen in figure (4.3a) that the number of calculated P_{CJ} that falls within ±5% of the experimental values are overall similar. The number ranges between 9 and 11 out of 14 conformers. The average deviation of eq. (1) for each level of theory is 1.83%, -1.03% and 1.99% for B3PW91/6-31G**, M06-2X/6-31G** and M06-2X/Jun-cc-pVTZ respectively. The maximum deviation of all P_{CJ} using eq. (1) is 7.46% and -8.52%. The P_{CJ} calculated using EXPLO5 seems to be underestimated when compared to the experimental value. The average deviation being -2.31%, -4.36% and -1.89% for B3PW91/6-31G**, M06-2X/6-31G** and M06-2X/Jun-cc-pVTZ respectively. The maximum of all these deviations being 0.83% and -11.27% thus suggesting an overall trend of underestimating the detonation pressure when compared to eq. (1). Analyzing the results from the mixtures further supports the trend of EXPLO5 underestimating the detonation pressure. The average deviation of Cyclotol and Comp B-3, using 5 different conformers of RDX, and Octol, using 3 conformers of HMX, was 1.37%, -2.78% and 0.56% from the experimental values using eq. (1) for B3PW91/6-31G**, M06-2X/6-31G** and M06-2X/Jun-cc-pVTZ respectively, see table 4. The number of calculated P_{CJ} using eq. (1) that falls within ±5% ranges from 11 to 13 out of 13. The resulting

average deviations of P_{CJ} using EXPLO5 is -6.59%, -10.17% and -7.57% for B3PW91/6-31G**, M06-2X/6-31G** and M06-2X/Jun-cc-pVTZ respectively. Only 0 to 2 calculated values fall within ±5% with the maximum deviations being -4.18% and -13.31%.

The overall pattern seems to be that the calculated P_{CJ} using M06-2X/6-31G**, for both eq. (1) and EXPLO5, are in the lower range of the total range of calculated P_{CJ} for the pure substances. However, for the mixtures using M06-2X/6-31G** in eq. (1) produced P_{CJ} in the upper range while EXPLO5 remained in the lower range.

4.4 Detonation Velocity

Another pattern emerges when analyzing the calculated detonation velocities. EXPLO5 seems to produce more accurate predictions of the detonation velocity. The largest deviations from the experimental value was 2.70% and -2.79% for both the pure substances and the mixtures, see figure (4.3b), table 3 and table 4.

A larger spread of calculated detonation velocities was produced using eq. (2) when compared to EXPLO5, ranging between 6.50% and -5.19%. However, these are overall accurate predictions of detonation velocities. Similarly to the calculated P_{CJ}, the trend seems to be that M06-2X/6-31G** predicts detonation velocities in the lower end of the range and M06-2X/Jun-cc-pVTZ in the upper end of the range.

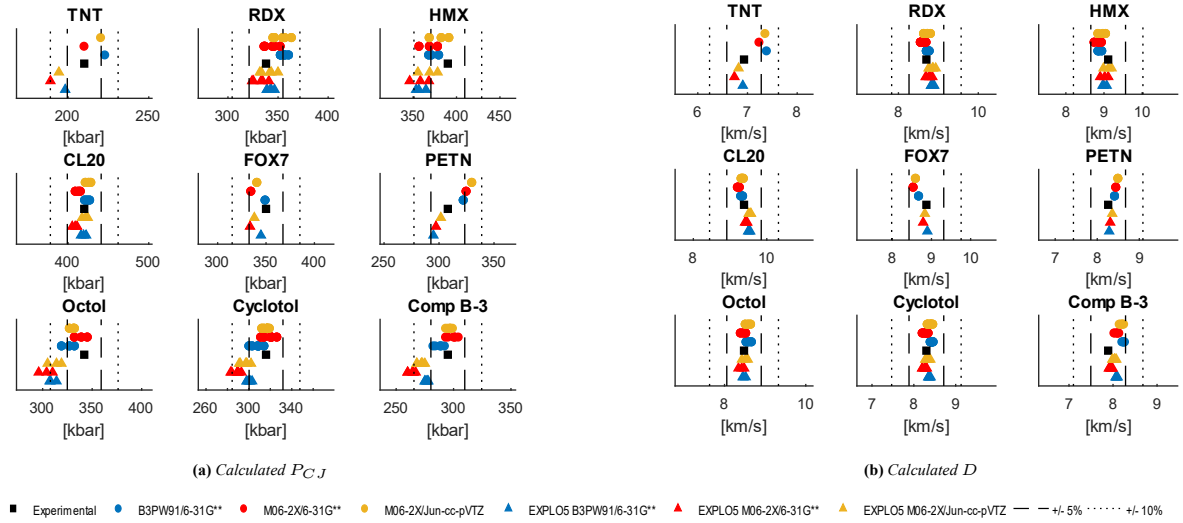

(a) *Calculated* P_{CJ} **(b)** *Calculated* D

Table 2. *Calculated P_{CJ} using Eq. (1) and EXPLO5 with their relative difference to their respective experimental detonation pressures.*

Experimental data			Calculated P_{CJ}			
Conformer	Detonation Pressure [kbar]	Functional/basis-set	Eq. (1) [kbar]	Rel. Diff	EXPLO5 [kbar]	Rel. Diff
TNT	210	B3PW91/6-31G**	223	6.0%	198	-5.6%
		M06-2X/6-31G**	210	-0.1%	189	-10.0%
		M06-2X/Jun-cc-pVTZ	220	4.8%	194	-7.5%
RDX α	338	B3PW91/6-31G**	356	5.3%	342	1.2%
		M06-2X/6-31G**	344	1.9%	333	-1.5%
		M06-2X/Jun-cc-pVTZ	355	5.0%	342	1.1%
RDX β	338	B3PW91/6-31G**	360	6.6%	346	2.5%
		M06-2X/6-31G**	352	4.2%	341	0.8%
		M06-2X/Jun-cc-pVTZ	363	7.5%	350	3.5%
RDX (I)	338	B3PW91/6-31G**	357	5.6%	343	1.6%
		M06-2X/6-31G**	346	2.4%	335	-1.0%
		M06-2X/Jun-cc-pVTZ	356	5.5%	343	1.6%
RDX (II)	338	B3PW91/6-31G**	352	4.3%	339	0.3%
		M06-2X/6-31G**	337	-0.3%	325	-3.7%
		M06-2X/Jun-cc-pVTZ	346	2.5%	333	-1.4%
RDX (III)	338	B3PW91/6-31G**	352	4.2%	339	0.3%
		M06-2X/6-31G**	336	-0.6%	324	-4.1%
		M06-2X/Jun-cc-pVTZ	345	2.0%	332	-1.8%
HMX (I)	390	B3PW91/6-31G**	368	-5.7%	354	-9.4%
		M06-2X/6-31G**	369	-5.4%	358	-8.1%
		M06-2X/Jun-cc-pVTZ	382	-2.0%	369	-5.4%
HMX β	390	B3PW91/6-31G**	371	-4.9%	357	-8.6%
		M06-2X/6-31G**	357	-8.5%	346	-11.3%
		M06-2X/Jun-cc-pVTZ	369	-5.5%	356	-8.8%
HMX δ	390	B3PW91/6-31G**	379	-2.7%	365	-6.5%
		M06-2X/6-31G**	378	-3.1%	368	-5.6%
		M06-2X/Jun-cc-pVTZ	391	0.3%	378	-3.0%
CL20 (I)	420	B3PW91/6-31G**	424	0.8%	419	-0.2%
		M06-2X/6-31G**	413	-1.8%	409	-2.7%
		M06-2X/Jun-cc-pVTZ	425	1.3%	422	0.4%
CL20 (II)	420	B3PW91/6-31G**	427	1.6%	409	-2.7%
		M06-2X/6-31G**	415	-1.2%	411	-2.1%
		M06-2X/Jun-cc-pVTZ	428	1.9%	424	1.0%
CL20 (III)	420	B3PW91/6-31G**	420	0.1%	422	0.6%
		M06-2X/6-31G**	409	-2.7%	405	-3.5%
		M06-2X/Jun-cc-pVTZ	421	0.3%	417	-0.6%
FOX7	350	B3PW91/6-31G**	349	-0.3%	345	-1.5%
		M06-2X/6-31G**	334	-4.5%	333	-4.7%
		M06-2X/Jun-cc-pVTZ	340	-2.7%	338	-3.5%
PETN	308	B3PW91/6-31G**	322	4.5%	295	-4.3%
		M06-2X/6-31G**	325	5.4%	297	-3.5%
		M06-2X/Jun-cc-pVTZ	330	7.0%	302	-2.1%
Average Deviation		B3PW91/6-31G**		1.83%		-2.31%
		M06-2X/6-31G**		-1.03%		-4.36%
		M06-2X/Jun-cc-pVTZ		1.99%		-1.89%

Table 3. *Calculated D using Eq. (2) and EXPLO5 with their relative difference to their respective experimental detonation velocities.*

Experimental data			Calculated D			
Conformer	Detonation Pressure $[km/s]$	Functional/basis-set	Eq. (2) $[km/s]$	Rel. Diff	EXPLO5 $[km/s]$	Rel. Diff
		B3PW91/6-31G**	7.38	6.5%	6.91	-0.3%
TNT	6.93	M06-2X/6-31G**	7.23	4.4%	6.74	-2.8%
		M06-2X/Jun-cc-pVTZ	7.35	6.1%	6.82	-1.6%
		B3PW91/6-31G**	8.73	0.3%	8.85	1.8%
RDX α	8.70	M06-2X/6-31G**	8.62	-0.9%	8.77	0.8%
		M06-2X/Jun-cc-pVTZ	8.72	0.2%	8.85	1.8%
		B3PW91/6-31G**	8.77	0.8%	8.90	2.3%
RDX β	8.70	M06-2X/6-31G**	8.69	-0.1%	8.85	1.7%
		M06-2X/Jun-cc-pVTZ	8.80	1.1%	8.93	2.7%
		B3PW91/6-31G**	8.74	0.5%	8.86	1.9%
RDX (I)	8.70	M06-2X/6-31G**	8.64	-0.7%	8.79	1.0%
		M06-2X/Jun-cc-pVTZ	8.73	0.4%	8.87	1.9%
		B3PW91/6-31G**	8.70	0.0%	8.82	1.4%
RDX (II)	8.70	M06-2X/6-31G**	8.55	-1.7%	8.70	0.0%
		M06-2X/Jun-cc-pVTZ	8.64	-0.7%	8.77	0.8%
		B3PW91/6-31G**	8.70	0.0%	8.82	1.3%
RDX (III)	8.70	M06-2X/6-31G**	8.55	-1.8%	8.68	-0.2%
		M06-2X/Jun-cc-pVTZ	8.63	-0.8%	8.76	0.6%
		B3PW91/6-31G**	8.84	-3.0%	8.96	-1.6%
HMX (I)	9.11	M06-2X/6-31G**	8.85	-2.9%	9.02	-1.0%
		M06-2X/Jun-cc-pVTZ	8.97	-1.6%	9.11	0.0%
		B3PW91/6-31G**	8.87	-2.7%	8.99	-1.3%
HMX β	9.11	M06-2X/6-31G**	8.74	-4.1%	8.90	-2.3%
		M06-2X/Jun-cc-pVTZ	8.84	-2.9%	8.99	-1.3%
		B3PW91/6-31G**	8.94	-1.9%	9.07	-0.4%
HMX δ	9.11	M06-2X/6-31G**	8.93	-2.0%	9.11	0.0%
		M06-2X/Jun-cc-pVTZ	9.04	-0.7%	9.20	1.0%
		B3PW91/6-31G**	9.32	-0.6%	9.52	1.5%
CL20 (I)	9.38	M06-2X/6-31G**	9.23	-1.6%	9.44	0.7%
		M06-2X/Jun-cc-pVTZ	9.33	-0.5%	9.54	1.8%
		B3PW91/6-31G**	9.34	-0.4%	9.55	1.8%
CL20 (II)	9.38	M06-2X/6-31G**	9.25	-1.4%	9.47	0.9%
		M06-2X/Jun-cc-pVTZ	9.36	-0.2%	9.57	2.0%
		B3PW91/6-31G**	9.29	-0.9%	9.49	1.2%
CL20 (III)	9.38	M06-2X/6-31G**	9.20	-2.0%	9.41	0.3%
		M06-2X/Jun-cc-pVTZ	9.30	-0.8%	9.51	1.3%
		B3PW91/6-31G**	8.67	-2.3%	8.90	0.3%
FOX7	8.87	M06-2X/6-31G**	8.53	-3.8%	8.79	-0.9%
		M06-2X/Jun-cc-pVTZ	8.59	-3.2%	8.83	-0.4%
		B3PW91/6-31G**	8.41	1.9%	8.28	0.3%
PETN	8.26	M06-2X/6-31G**	8.44	2.2%	8.31	0.6%
		M06-2X/Jun-cc-pVTZ	8.49	2.7%	8.36	1.2%
		B3PW91/6-31G**		-0.62%		0.47%
Average Deviation		M06-2X/6-31G**		-1.63%		-0.33%
		M06-2X/Jun-cc-pVTZ		-0.60%		0.54%

Table 4. *Calculated P_{CJ} and D using Eq. (1), Eq. (2) and EXPLO5 of the mixtures with their relative difference to their respective experimental data.*

Composition	Conformer	Exp.	Eq. (1)						EXPLO5					
			B3PW91		M06-2X		M06-2X		B3PW91		M06-2X		M06-2X	
			6-31G**		6-31G**		Jun-cc-pVTZ		6-31G**		6-31G**		Jun-cc-pVTZ	
		[$kbar$]	[$kbar$]	Diff	[$kbar$]	Diff	[$kbar$]	Diff	[$kbar$]	Diff	[$kbar$]	Diff	[$kbar$]	Diff
Comp B3	RDX α	295	304	2.95%	289	-2.05%	301	1.88%	276	-6.35%	264	-10.56%	272	-7.90%
	RDX β	295	306	3.73%	293	-0.74%	305	3.23%	278	-5.65%	267	-9.38%	275	-6.63%
	RDX (I)	295	304	3.02%	290	-1.85%	301	2.08%	277	-6.14%	265	-10.29%	272	-7.63%
	RDX (II)	295	302	2.23%	285	-3.54%	296	0.33%	275	-6.84%	260	-11.70%	268	-9.13%
	RDX (III)	295	300	1.77%	282	-4.24%	294	-0.40%	275	-6.84%	260	-11.78%	268	-9.31%
Cyclotol	RDX α	316	324	2.49%	309	-2.23%	321	1.56%	300	-5.07%	289	-8.70%	297	-6.12%
	RDX β	316	327	3.47%	314	-0.58%	326	3.27%	303	-4.18%	293	-7.15%	302	-4.46%
	RDX (I)	316	324	2.58%	310	-1.99%	322	1.81%	301	-4.83%	290	-8.36%	298	-5.78%
	RDX (II)	316	321	1.59%	303	-4.11%	315	-0.39%	298	-5.74%	284	-10.19%	292	-7.72%
	RDX (III)	316	319	1.01%	300	-4.98%	312	-1.30%	298	-5.76%	283	-10.37%	291	-8.03%
Octol	HMX (I)	342	327	-4.37%	340	-0.67%	332	-2.99%	307	-10.35%	304	-11.06%	314	-8.27%
	HMX β	342	335	-2.10%	320	-6.53%	332	-2.91%	308	-9.82%	296	-13.31%	305	-10.76%
	HMX δ	342	340	-0.52%	333	-2.64%	346	1.13%	314	-8.07%	310	-9.36%	319	-6.69%

Composition	Conformer	Exp.	Eq. (2)						EXPLO5					
			B3PW91		M06-2X		M06-2X		B3PW91		M06-2X		M06-2X	
			6-31G**		6-31G**		Jun-cc-pVTZ		6-31G**		6-31G**		Jun-cc-pVTZ	
		[km/s]	[km/s]	Diff	[km/s]	Diff	[km/s]	Diff	[km/s]	Diff	[km/s]	Diff	[km/s]	Diff
Comp B3	RDX α	7.89	8.08	2.42%	7.95	0.78%	8.03	1.82%	8.08	2.42%	7.95	0.78%	8.03	1.82%
	RDX β	7.89	8.10	2.70%	7.99	1.27%	7.99	1.27%	8.10	2.70%	7.99	1.27%	8.07	2.34%
	RDX (I)	7.89	8.09	2.50%	7.96	0.89%	7.96	0.89%	8.09	2.50%	7.96	0.89%	8.04	1.92%
	RDX (II)	7.89	8.06	2.21%	7.91	0.29%	7.91	0.29%	8.06	2.21%	7.91	0.29%	7.99	1.30%
	RDX (III)	7.89	8.06	2.21%	7.91	0.23%	7.91	0.23%	8.06	2.21%	7.91	0.23%	7.99	1.21%
Cyclotol	RDX α	8.30	8.43	1.58%	8.29	-0.15%	8.40	1.24%	8.37	0.86%	8.26	-0.50%	8.34	0.47%
	RDX β	8.30	8.46	1.94%	8.34	0.46%	8.45	1.86%	8.40	1.21%	8.31	0.12%	8.39	1.14%
	RDX (I)	8.30	8.43	1.61%	8.29	-0.06%	8.41	1.34%	8.38	0.95%	8.27	-0.37%	8.35	0.61%
	RDX (II)	8.30	8.40	1.25%	8.23	-0.85%	8.34	0.53%	8.35	0.59%	8.21	-1.12%	8.29	-0.18%
	RDX (III)	8.30	8.39	1.04%	8.20	-1.18%	8.32	0.19%	8.35	0.58%	8.20	-1.21%	8.27	-0.31%
Octol	HMX (I)	8.48	8.46	-0.22%	8.58	1.19%	8.51	0.31%	8.45	-0.38%	8.42	-0.67%	8.52	0.43%
	HMX β	8.48	8.53	0.65%	8.39	-1.05%	8.51	0.34%	8.47	-0.14%	8.34	-1.61%	8.43	-0.59%
	HMX δ	8.48	8.59	1.24%	8.52	0.44%	8.64	1.86%	8.52	0.49%	8.48	0.06%	8.57	1.09%

4.5 Comparison

The average of the calculated P_{CJ} and D of each energetic material compared with their respective experimental data can be seen in figure (4.4a) and (4.4c) respectively. The average of the calculated P_{CJ} and D for the new candidates are shown together with the traditional energetic materials in figure (4.4b) and (4.4d). Due to problems during the calculations of ONC with M06-2X/Jun-cc-pVTZ, its results could not be included in the averaging of the P_{CJ} and D. The overall pattern is the average P_{CJ} and D follows the experimental data fairly accurately and the over- and underestimations appears to be random.

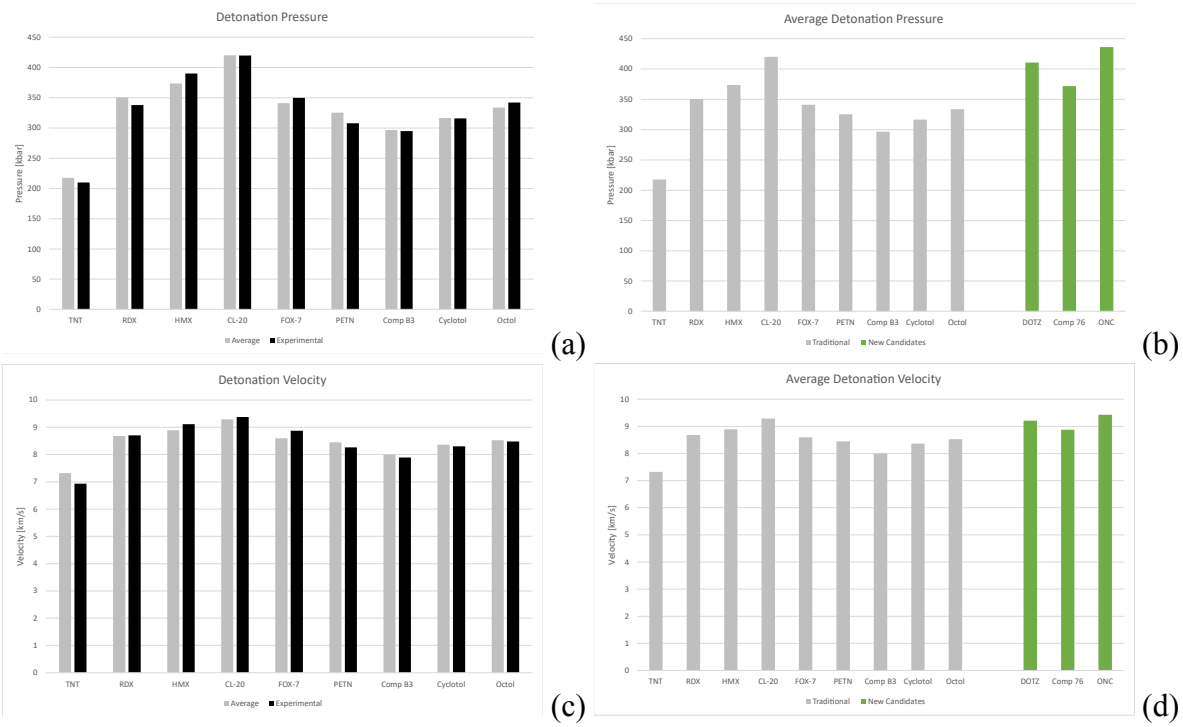

Figure 4.4: *Average calculated detonation pressure of traditional energetic materials compared with experimental data (a), average calculated detonation pressure of traditional and new energetic materials (b), average calculated detonation velocity of traditional energetic materials compared with experimental data (c), average calculated detonation velocity of traditional and new energetic materials (d).*

5 Discussion

Based on these results, this method seems to accurately predict P_{CJ} and D using eq. (1) and eq. (2). All of the calculated P_{CJ}'s were within $\pm 10\%$ of their respective experimental value and 71% of these were within $\pm 5\%$. All of the predicted D's were also within $\pm 10\%$ of their respective experimental value with an even narrower spread where 74% of these are within $\pm 2.5\%$. The difference in the spread of the calculated P_{CJ} and D using eq. (1) and eq. (2) can be explained by the nature of the equations. Since the P_{CJ} in eq. (1) is linearly dependent to $Q_{Det}^{1/2}\,\rho_0^2$ and D in eq. (2) is linearly dependent to $Q_{Det}^{1/4}\,\rho_0$, D will be less sensitive to a difference in Q_{Det} and ρ_0 than the P_{CJ}. No apparent pattern regarding certain functional groups can be seen. Comparing RDX and HMX, which are structurally similar, it can be seen that RDX is generally overestimated and HMX is underestimated when compared to their experimental values. This suggests that the predicted P_{CJ} does not follow a trend regarding structural similarity or functional groups. This is not surprising since eq. (1) is empirically developed from a diverse group of energetic materials. However, more structures needs to be evaluated in order to confidently state that this method is not biased towards certain molecular classes.

There is not a great difference between the different levels of theory. The overall trend regarding the heats of formation, and in turn Q_{Det}, is that the M06-2X/Jun-cc-pVTZ produce the most accurate results. B3PW91/6-31G** predicts less accurate heats of formation and M06-2X/6-31G** is the least accurate. However, this does not seem to have a great impact the end result since the average deviation of M06-2X/6-31G** and M06-2X/Jun-cc-pVTZ was -1.03% and 1.99% respectively. The small difference could be the result of the definition of Q_{Det} itself in eq. (3) where the difference between the heats of formation of the explosive and its products are divided by the molecular mass of the explosive. This reduces the impact of the heat of formation of the explosive. The impact is again reduces in eq. (1) where $P_{CJ} \propto \mathrm{Q}_{Det}^{1/2}$.

When it comes to the crystal densities the M06-2X functional predicts more accurately than the B3PW91 functional with their average estimations being 13 mg and 29 mg below the TMD's respectively. Since the Jun-cc-pVTZ basis-set is not parameterized in the HS95 code, the surface descriptors from M06-2X/6-31G** were used, thus a comparison between 6-31G** and Jun-cc-pVTZ regarding crystal density can not be performed. However, the geometries of these two levels of theory should share a high degree of resemblance since they both use

the same functional, which should result in an almost identical ESP and thus almost identical surface descriptors.

The new candidates showed promising detonations properties where all of them seems to outperform HMX while DOTZ almost outperforms CL20. ONC has the highest P_{CJ} and D out of the total investigated energetic materials.

Regarding the choice of which level of theory to use in further studies, the M06-2X/6-31G** level of theory would be the optimal choice when taking aspects like simplicity and computational cost into account. The method utilizing B3PW91/6-31G** requires some atomic correction terms when calculating the heats of formation in the gaseous state. This increases the complexity when performing calculations. When it comes to the computational cost of using the Jun-cc-pVTZ basis-set, it may not be worth the increased accuracy of the estimated heats of formation. M06-2X/6-31G** has therefore the best trade off between accuracy, simplicity and computational cost.

5.1 Final Words

As shown in this work, this method can be used to predict the detonation pressure and detonation velocity of energetic material with good accuracy. The choice of level of theory does not seem to impact the final result to a major extent. This makes M06-2X/6-31G** the most appropriate choice when considering the simplicity and computational cost.

5.2 Future Work

The detonation performance is not the only important factor when working with energetic materials. The sensitivity is also a major concern since unexpected detonations can be detrimental and is unacceptable. Unfortunately, high detonation performance and low sensitivity are often inversely proportional to one another. To be able to predict this property would also be highly valuable when designing new energetic materials. As of yet, this has been difficult to model and the best relationships that have been found only indicate relative trends. Since the sensitivity is related to several types of stimuli i.e impact, friction, heat and electric spark etc. there are several suggestions of what features play a role in the initiation of a detonation. One model involves ”trigger bonds”, which are bonds that it thought to initiate detonation. Adding different functional groups to the molecule can weaken or strengthen this trigger bond and thus increase or decrease the sensitivity. Bond strengths can be calculated using quantum chemical methods, this shows the wide applicability of quantum chemistry towards finding new energetic materials.

References

[1] Bondarchuk, Sergey V. “Modeling of explosives: 1,4,2,3,5,6-dioxatetrazinane as a new green energetic material with enhanced performance”. In: *Journal of Physics and Chemistry of Solids* 142 (July 2020), p. 109458. DOI: 10.1016/j.jpcs.2020.109458. (Visited on 06/14/2022).

[2] Brinck, Tore. *Green energetic materials*. Wiley, 2014, pp. 1–2.

[3] Brinck, Tore. *Green energetic materials*. Wiley, 2014, pp. 103–104.

[4] Brinck, Tore. *Green energetic materials*. Wiley, 2014, pp. 51–56.

[5] Eaton, P. E., Gilardi, R. L., and Zhang, M.-X. “Polynitrocubanes: Advanced High-Density, High-Energy Materials”. In: *Advanced Materials* 12 (Aug. 2000), pp. 1143–1148. DOI: 10.1002/1521-4095(200008)12:15<1143::aid-adma1143>3.0.co;2-5. (Visited on 06/14/2022).

[6] Keshavarz, Mohammad, Kamalvand, Mohammad, Jafari, Mohammad, and Zamani, Ahmad. “An Improved Simple Method for the Calculation of the Detonation Performance of CHNOFCl, Aluminized and Ammonium Nitrate Explosives”. In: *Central European Journal of Energetic Materials* 13 (2016), pp. 381–396. DOI: 10.22211/cejem/64991.

[7] Keshavarz, Mohammad Hossein and Pouretedal, Hamid Reza. “An empirical method for predicting detonation pressure of CHNOFCl explosives”. In: *Thermochimica Acta* 414 (May 2004), pp. 203–208. DOI: 10.1016/j.tca.2003.11.019.

[8] Long, Bryan A., Lau, Chris Y., Rodriguez, Daniel J., Tang, Susanna An, and Anderson, Scott L. “Sublimation Kinetics for Individual Graphite and Graphene Nanoparticles (NPs): NP-to-NP Variations and Evolving Structure-Kinetics and Structure-Emissivity Relationships”. In: *Journal of the American Chemical Society* 142 (July 2020), pp. 14090–14101. DOI: 10.1021/jacs.0c01720. (Visited on 05/28/2022).

[9] Molt, Robert W., Watson, Thomas, Bazanté, Alexandre P., and Bartlett, Rodney J. “The Great Diversity of HMX Conformers: Probing the Potential Energy Surface Using CCSD(T)”. In: *The Journal of Physical Chemistry A* 117 (Apr. 2013), pp. 3467–3474. DOI: 10.1021/jp311073m.

[10] Molt, Robert W., Watson, Thomas, Lotrich, Victor F., and Bartlett, Rodney J. “RDX Geometries, Excited States, and Revised Energy Ordering of Conformers via MP2 and CCSD(T) Methodologies: Insights into Decomposition Mechanism”. In: *The Journal of Physical Chemistry A* 115 (Jan. 2011), pp. 884–890. DOI: 10.1021/jp109695v.

[11] Politzer, Peter, Ma, Yuguang, Lane, Pat, and Concha, Monica C. “Computational prediction of standard gas, liquid, and solid-phase heats of formation and heats of vaporization and sublimation”. In: *International Journal of Quantum Chemistry* 105 (2005), pp. 341–347. DOI: 10.1002/qua.20709.

[12] Politzer, Peter, Martinez, Jorge, Murray, Jane S., Concha, Monica C., and Toro-Labbé, Alejandro. “An electrostatic interaction correction for improved crystal density prediction”. In: *Molecular Physics* 107 (Oct. 2009), pp. 2095–2101. DOI: 10.1080/00268970903156306.

[13] Ye, Cai-Chao, An, Qi, Zhang, Wen-Qing, and Goddard, William A. “Initial Decomposition of HMX Energetic Material from Quantum Molecular Dynamics and the Molecular Structure Transition of β-HMX to δ-HMX”. In: *The Journal of Physical Chemistry C* 123 (Mar. 2019), pp. 9231–9236. DOI: 10.1021/acs.jpcc.9b01169.

[14] Zhou, Jing, Zhang, Junlin, Wang, Bozhou, Qiu, Lili, Xu, Ruoqian, and Sheremetev, Aleksei B. “Recent synthetic efforts towards high energy density materials: How to design high-performance energetic structures?” In: *FirePhysChem* 2 (June 2022), pp. 83–139. DOI: 10.1016/j.fpc.2021.09.005. (Visited on 06/14/2022).

Appendix

Table A. *Table containing the obtained surface descriptors, heats of sublimation and crystal densities of the traditional energetic materials.*

Surface descriptors									
Conformer	Functional/basis-set	A_S	$\sigma^2{}_+$	$\sigma^2{}_-$	V	σ^2_{tot}	$\boldsymbol{\nu}$	ΔH_{Sub}	ρ_0
TNT	B3PW91/6-31G**	212.15	58.86	30.90	219.78	89.76	0.2257	26.73	1.6769
TNT	M06-2X/6-31G**	211.99	61.80	32.10	220.32	93.90	0.2250	26.90	1.6755
TNT	M06-2X/Jun-cc-pVTZ	211.99	61.80	32.10	220.32	93.90	0.2250	26.90	1.6755
RDX α	B3PW91/6-31G**	196.31	163.17	38.31	202.37	201.48	0.1540	26.07	1.8049
RDX α	M06-2X/6-31G**	193.47	177.05	43.45	202.02	220.50	0.1582	26.27	1.8186
RDX α	M06-2X/Jun-cc-pVTZ	193.47	177.05	43.45	202.02	220.50	0.1582	26.27	1.8186
RDX β	B3PW91/6-31G**	193.89	143.31	43.49	201.80	186.80	0.1786	26.07	1.8162
RDX β	M06-2X/6-31G**	188.65	152.34	51.81	200.87	204.15	0.1894	26.09	1.8388
RDX β	M06-2X/Jun-cc-pVTZ	188.65	152.34	51.81	200.87	204.15	0.1894	26.09	1.8388
RDX (I)	B3PW91/6-31G**	194.34	113.09	38.67	201.51	151.76	0.1899	25.31	1.8058
RDX (I)	M06-2X/6-31G**	190.05	109.96	43.29	200.38	153.25	0.2027	25.00	1.8216
RDX (I)	M06-2X/Jun-cc-pVTZ	190.05	109.96	43.29	200.38	153.25	0.2027	25.00	1.8216
RDX (II)	B3PW91/6-31G**	199.44	171.36	34.04	202.75	205.40	0.1383	26.12	1.7944
RDX (II)	M06-2X/6-31G**	197.67	185.30	34.21	202.76	219.51	0.1316	25.90	1.7956
RDX (II)	M06-2X/Jun-cc-pVTZ	197.67	185.30	34.21	202.76	219.51	0.1316	25.90	1.7956
RDX (III)	B3PW91/6-31G**	201.59	168.19	31.94	203.03	200.13	0.1341	26.20	1.7877
RDX (III)	M06-2X/6-31G**	200.41	176.66	30.62	203.12	207.28	0.1259	25.84	1.7849
RDX (III)	M06-2X/Jun-cc-pVTZ	200.41	176.66	30.62	203.12	207.28	0.1259	25.84	1.7849
HMX (I)	B3PW91/6-31G**	232.57	94.87	32.93	263.05	127.80	0.1913	31.67	1.8296
HMX (I)	M06-2X/6-31G**	218.31	79.01	46.53	256.92	125.54	0.2333	29.78	1.8841
HMX (I)	M06-2X/Jun-cc-pVTZ	218.31	79.01	46.53	256.92	125.54	0.2333	29.78	1.8841
HMX β	B3PW91/6-31G**	239.37	177.50	38.90	264.57	216.40	0.1474	34.54	1.8406
HMX β	M06-2X/6-31G**	232.38	171.01	41.23	262.81	212.24	0.1565	33.32	1.8557
HMX β	M06-2X/Jun-cc-pVTZ	232.38	171.01	41.23	262.81	212.24	0.1565	33.32	1.8557
HMX δ	B3PW91/6-31G**	239.66	230.47	49.38	265.33	279.85	0.1453	36.10	1.8602
HMX δ	M06-2X/6-31G**	225.30	195.52	64.79	261.63	260.31	0.1869	34.38	1.9067
HMX δ	M06-2X/Jun-cc-pVTZ	225.30	195.52	64.79	261.63	260.31	0.1869	34.38	1.9067
FOX7	B3PW91/6-31G**	146.03	335.10	108.52	139.33	443.62	0.1848	25.62	1.8945
FOX7	M06-2X/6-31G**	146.66	350.56	108.57	139.88	459.13	0.1806	25.80	1.8907
FOX7	M06-2X/Jun-cc-pVTZ	146.66	350.56	108.57	139.88	459.13	0.1806	25.80	1.8907
CL20 (I)	B3PW91/6-31G**	308.09	213.17	16.40	354.08	229.57	0.0663	47.61	1.9741
CL20 (I)	M06-2X/6-31G**	299.31	217.70	18.44	351.65	236.14	0.0720	45.70	1.9921
CL20 (I)	M06-2X/Jun-cc-pVTZ	299.31	217.70	18.44	351.65	236.14	0.0720	45.70	1.9921
CL20 (II)	B3PW91/6-31G**	306.55	205.41	17.47	353.14	222.88	0.0722	47.42	1.9815
CL20 (II)	M06-2X/6-31G**	297.65	214.17	19.44	350.66	233.61	0.0763	45.47	1.9997
CL20 (II)	M06-2X/Jun-cc-pVTZ	297.65	214.17	19.44	350.66	233.61	0.0763	45.47	1.9997
CL20 (III)	B3PW91/6-31G**	309.49	220.41	14.79	354.8	235.2	0.0589	47.63	1.9664
CL20 (III)	M06-2X/6-31G**	300.34	216.81	16.02	352.67	232.83	0.0641	45.44	1.9807
CL20 (III)	M06-2X/Jun-cc-pVTZ	300.34	216.81	16.02	352.67	232.83	0.0641	45.44	1.9807
PETN	B3PW91/6-31G**	283.13	107.18	15.39	287.27	122.57	0.1098	40.59	1.7601
PETN	M06-2X/6-31G**	281.83	118.27	16.78	286.87	135.05	0.1088	40.61	1.7659
PETN	M06-2X/Jun-cc-pVTZ	281.83	118.27	16.78	286.87	135.05	0.1088	40.61	1.7659

TRITA-CBH-GRU-2022:224